Precision analysis of $\Lambda_{\overline{\rm MS}}$ and the gluon distribution and its implications for jet and top-quark cross sections

A. D. Martin
Department of Physics, University of Durham, Durham DH1 3LE, England

R. G. Roberts
Rutherford Appleton Laboratory, Chilton, Didcot OX11 0QX, England

W. J. Stirling*
Department of Physics, University of Washington, Seattle Washington 98195
(Received 8 November 1990)

Recent deep-inelastic and prompt-photon data are used to put quantitative limits on $\Lambda_{\overline{\rm MS}}$ (where $\overline{\rm MS}$ denotes the modified minimal-subtraction scheme) and the gluon distribution, taking fully into account the correlations between the two. The results are used (a) to assess the potential discriminating power of precision measurements of the large-transverse-momentum jet cross section at the Fermilab $p\bar{p}$ collider, and (b) to estimate the theoretical error on a top-quark-mass measurement or lower limit at the same collider. We estimate this latter error at approximately ± 4 GeV at present, with the prospect of some slight improvement from an additional calibration from the jet cross section.

I. INTRODUCTION

A reliable and precise set of parton distributions, together with a precise value of strong coupling α_s, is of fundamental importance in applying perturbative QCD to a wide range of hard-scattering processes in hadronic collisions. Apart from wishing to test the consistency of the theory itself over this range of applications, it is crucial to have a precise knowledge of the distributions and of the parameter $\Lambda_{\overline{\rm MS}}$ (where $\overline{\rm MS}$ denotes the modified minimal-subtraction scheme) in order to extract other information from a given reaction. An example is the hadronic production of W and Z at $p\bar{p}$ colliders, where only the product of the cross section and the branching ratio can be measured. Since the former is entirely specified in terms of the quark and gluon distributions and α_s, a precise and dependable knowledge of these allows important information to be extracted from the branching ratios (in particular, limits on the number of light neutrinos and on m_t). Even the measurement of the W mass depends on precisely known parton distributions.[1]

Analyzing precise measurements in deep-inelastic lepton-hadron scattering[2-4] combined with those from hadronic production of prompt photons[5] and dimuons[6] leads to reliable sets of parton distributions and of values of $\Lambda_{\overline{\rm MS}}$.[7] Distributions which are valid to very small values of x are now available[8] and can be used to predict the new kinematic region to be opened up by the ep collider HERA at DESY. While these sets provide "standard" distributions, which may be used in applying perturbative QCD to a particular process, it is important to have some measure of the uncertainty associated with them and with the value of $\Lambda_{\overline{\rm MS}}$. This paper attempts to provide such realistic limits which will in turn allow other quantities to be extracted from any process with proper estimates of the resulting errors on that quantity. This will then replace the rather *ad hoc* procedure of estimating those errors from the variation resulting from simply using in turn all sets of distributions (some of which are inconsistent with current data) that are available.

In Sec. II we carefully examine the fits to deep-inelastic data and prompt photon production and, in particular, the role they play in pinning down the precise value of $\Lambda_{\overline{\rm MS}}$ and the shape of the gluon distribution. From these fits we produce, in addition to the standard fit, four "extreme" fits which reflect the maximum allowable variations of $\Lambda_{\overline{\rm MS}}$ and η_g, the exponent of $(1-x)$ in the gluon distribution.

One reason for demanding better estimates of the uncertainties in the parton distributions, and in α_s, is the steady improvement in the precision both of the data itself and of the theoretical description of the relevant processes. A beautiful illustration of such a process is inclusive jet production at the $p\bar{p}$ colliders. Recently, the CDF Collaboration[9] at the Fermilab $p\bar{p}$ collider have measured the jet p_T distribution—data which span seven decades as p_T goes from 40 to 400 GeV/c—and, in addition, the next-to-leading-order (NLO) perturbative QCD corrections have been calculated by Ellis, Kunszt, and Soper.[10] In Sec. III A we obtain our central and extreme predictions for this process and discuss how different ranges of p_T reflect the different characteristics of the five sets of partons. From this one can assess how precise measurements of jet production could be used to discriminate between the different parton solutions, and therefore yield information on $\Lambda_{\overline{\rm MS}}$ and η_g.

Another process which requires precise limits on the allowed variation of the distributions is the production of

the top quark at the $p\bar{p}$ colliders. Since the event rate is not expected to be large, the top mass will be determined by comparing the measured cross section (or cross-section upper limit if no events are observed) with the theoretical prediction as a function of m_t. We examine, in Sec. III B, the sensitivity of the value of m_t extracted in this way to the uncertainties in $\Lambda_{\overline{\rm MS}}$, the shape of the input gluon distributions at $Q_0^2 = 4$ GeV^2, and the evolution of the quark distributions resulting from different values of $\Lambda_{\overline{\rm MS}}$. Thus when the top quark is eventually discovered, the uncertainty in m_t resulting from the parton distributions can be properly estimated.

II. DETERMINATION OF $\Lambda_{\overline{\rm MS}}$ AND THE GLUON

In earlier work[7,8] we have presented next-to-leading-order QCD analyses of deep-inelastic and related data. In each case the parton distributions were parametrized by some functional form at $Q_0^2 = 4$ GeV^2 (using a total of about a dozen parameters) and evolved in Q^2 using the fitted value of $\Lambda_{\overline{\rm MS}}$. In Ref. 7 we produced two solutions—HMRS(B) and HMRS(E)—according to whether the BCDMS (Ref. 2) or EMC (Ref. 4) $F_2^{\mu p}$ data were used as input. In fact both were renormalized overall to match up with the recent SLAC data[11] at low Q^2, so that the discrepancy between them was less marked, being significant only at large x. Special attention was given to the small-x region in Ref. 8, where we derived two solutions B_0 and B_- depending on whether the input gluon distribution (times x) at Q_0^2 was finite or singular as $x \to 0$; that is, with

$$xg(x, Q_0^2) \longrightarrow x^\lambda, \tag{1}$$

where λ was either zero or $-\frac{1}{2}$, but one had to go to x below 0.002–0.005 to see any significant deviation between the two. Since in this paper we are not concerned with very small x we can simply take the B_0 solution as our "central" fit. Note that except at small x the HMRS(B) and B_0 distributions are only marginally different, and therefore give essentially identical results for the cross sections discussed below.

In this section we examine how the two parameters $\Lambda_{\overline{\rm MS}}$ and η_g are constrained by the data. First, we omit the prompt-photon data from the fit, i.e., we include the deep-inelastic data on $F_2^{\mu p}$—renormalized by 0.98—from BCDMS,[2] on $F_{2,3}^{\nu N}$ from CDHSW[3] and on $F_2^{\mu n}/F_2^{\mu p}$ from NMC, BCDMS, and EMC.[12] Altogether there are 352 data points, and in Fig. 1 we show the χ^2 obtained by fitting these data with the values of $\Lambda_{\overline{\rm MS}}$ and η_g shown. In each data set we add the statistical and systematic errors in quadrature. The location of the central B_0 fit ($\eta_g = 5.1, \Lambda_{\overline{\rm MS}} = 190$ MeV) is marked. Note that for $\Lambda_{\overline{\rm MS}} \gtrsim 180$ MeV there is a definite *anticorrelation* between $\Lambda_{\overline{\rm MS}}$ and η_g.

We next include the prompt-photon data from WA70[5] and in Fig. 2 show the resulting χ^2 contours obtained from the eight data points of $d\sigma/dp_T^\gamma(pp \to \gamma X)$ as a

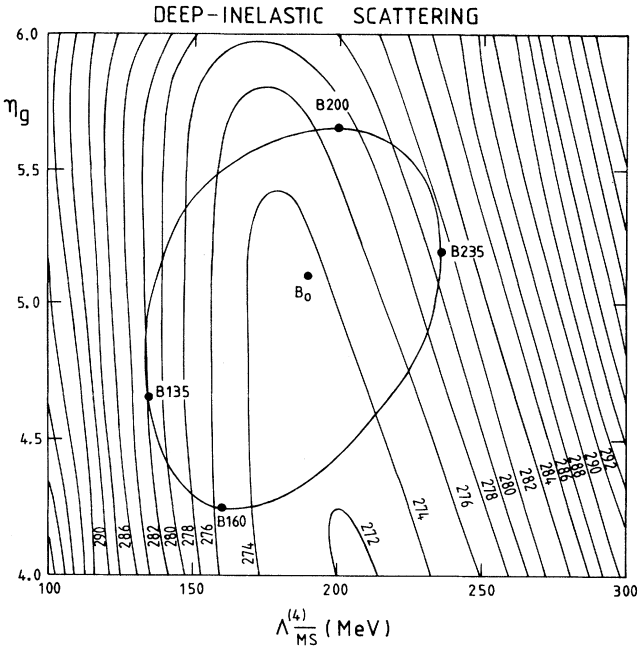

FIG. 1. Contours of the χ^2 values resulting from fits to the 352 points of deep-inelastic data (Refs. 2, 3, and 12) for given values of $\Lambda_{\overline{\rm MS}}$ and η_g. The superimposed ellipse-like closed contour corresponds to $\chi^2_{\rm min} + 10$ where $\chi^2_{\rm min}$ is the overall minimum χ^2 from the fit to the combined deep-inelastic and prompt-photon data set. The four sets of partons corresponding to the points B135, B160, B200, B235 are taken to be representative of the spread of uncertainty in the parton distributions. The "best fit" set of partons, B_0 is as described in Ref. 8.

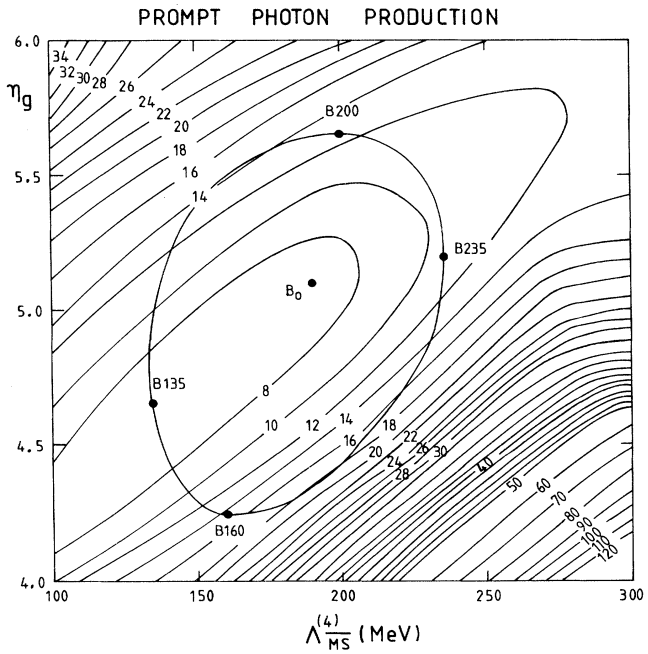

FIG. 2. Contours of the χ^2 values resulting from fits to the 8 points of prompt photon production data (Ref. 5) for given values of $\Lambda_{\overline{\rm MS}}$ and η_g. The ellipselike contour is exactly as in Fig. 1.

function of η_g and $\Lambda_{\overline{\rm MS}}$. Again the statistical and systematic errors on the data are combined in quadrature. As in our previous analysis,[7] the theoretical cross section is calculated to next-to-leading order using optimization to determine the factorization and renormalization scales. Now we see a *correlation* between the two parameters and a steep minimum in χ^2 which is approximately in the direction orthogonal to that in Fig. 1 (see also Ref. 13). Again we show the values corresponding to the central (B_0) fit.

From Figs. 1 and 2 we can see that precise determinations of the two parameters are possible only if the prompt-photon data are combined with the deep-inelastic data. Figure 3 illustrates the effect of taking the BCDMS $F_2^{\mu p}$ data alone (142 points) compared to the full data set. The χ^2 at fixed values of η_g is plotted versus $\Lambda_{\overline{\rm MS}}$ and one sees the relatively broad minimum which obtains when only the μp data are included. The anticorrelation between η_g and $\Lambda_{\overline{\rm MS}}$ in this case also results in a significant shift in the value of $\Lambda_{\overline{\rm MS}}$ depending on whether η_g is taken as 5 or 10. We conclude that the BCDMS data on their own are unable to give a precise determination of η_g which, in turn, gives some extra uncertainty in the measurement of $\Lambda_{\overline{\rm MS}}$ using just these data.

In Figs. 1 and 2 we also display the contour of $\chi^2 = \chi^2_{\rm min} + 10$ where $\chi^2_{\rm min}$ is the minimum *combined* χ^2 to the complete deep-inelastic and prompt-photon data set. We take this contour to mark the limit of acceptable fits to the data. On this boundary we choose four points in the $\eta_g, \Lambda_{\overline{\rm MS}}$ plane corresponding to extreme values of the two parameters, as given by

$$\Lambda^{(4)}_{\overline{\rm MS}} = 185 \pm 50 \text{ MeV}, \qquad \eta_g = 4.95 \pm 0.7. \tag{2}$$

These fits we label as B135, B160, B200, and B235 (the number denoting the value of $\Lambda^{(4)}_{\overline{\rm MS}}$) and summarize, together with B_0, in Table I. The errors we quote in Eq. (2) are not true errors in the $\pm 1\sigma$ sense. Although our method of assigning errors according to the $\Delta\chi^2 = 10$ criterion is necessarily somewhat subjective, the fact that the range of solutions we consider does indeed span the data with a reasonable standard deviation is illustrated in Fig. 4, where we show the fits to the WA70 prompt-photon data for all four BΛ sets of partons, relative to B_0.

From Fig. 4 we see, as expected, that the *shape* of the resulting p_T^γ distribution is governed by the shape of the gluon distribution, i.e., by η_g, while the overall *nor-*

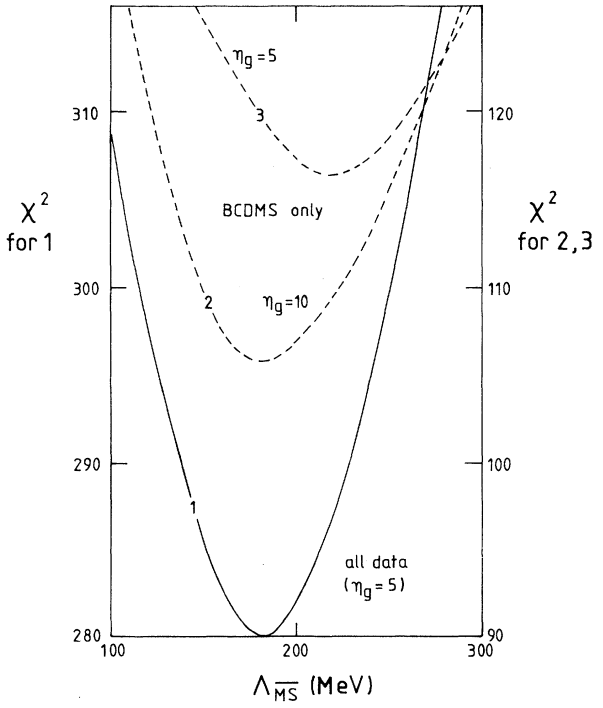

FIG. 3. Variation of χ^2 with $\Lambda_{\overline{\rm MS}}$ at fixed values of η_g. The continuous curve is obtained from the fit to all 360 points of deep-inelastic and prompt-photon data with $\eta_g = 5$. The dashed curves 2 and 3 correspond to fits to just the 142 BCDMS $F_2^{\mu p}$ data points (Ref. 2) with $\eta_g = 10$ and 5, respectively, where the χ^2 scale is shown on the right-hand side.

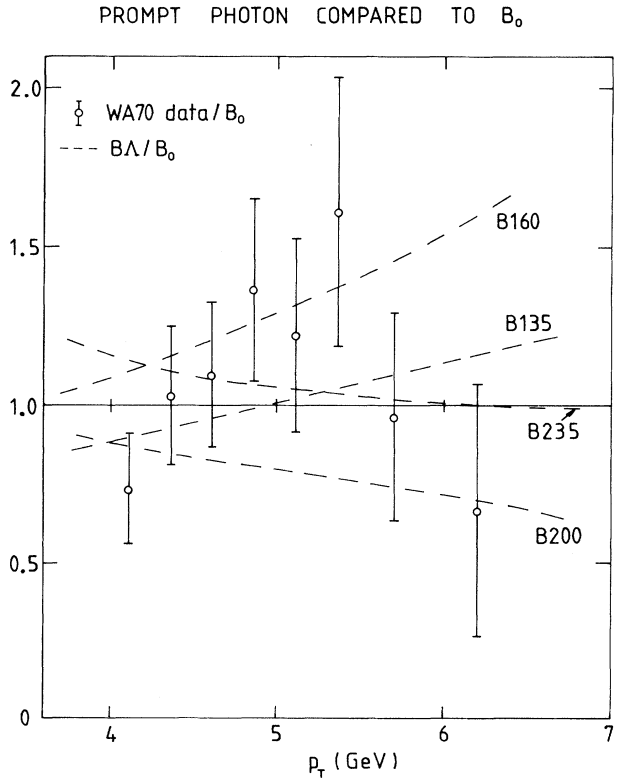

FIG. 4. The description of the prompt-photon data of Ref. 5 obtained from the five sets of partons in Table I normalized to the central B_0 fit.

TABLE I. Parameters associated with the fits discussed in the text.

Set	$\Lambda^{(4)}_{\overline{\rm MS}}$ (MeV)	$\Lambda^{(5)}_{\overline{\rm MS}}$ (MeV)	η_g	$\alpha_s(M_Z)$
B_0	190	124	5.10	0.1091
B135	135	85	4.65	0.1037
B160	160	102	4.25	0.1063
B200	200	131	5.65	0.1100
B235	235	156	5.20	0.1128

malization is determined by the magnitude of α_s. Note that if, following Ref. 13, we were to omit the WA70 data point at the lowest value of p_T^γ then slightly larger values of $\Lambda_{\overline{\rm MS}}$ are favored. We would find that the combined deep-inelastic and prompt-photon data then give $\Lambda^{(4)}_{\overline{\rm MS}} = 195 \pm 55$ MeV.

We propose that the four parton sets $B\Lambda$ = B135, B160, B200, B235 of Table I can be used to obtain realistic limits to the uncertainty of our central solution B_0. (The five sets of parton distributions can be obtained by electronic mail from WJS@UK.AC.DUR.HEP or 19681::WJS.) In the next section we show how these may be applied in a quantitative analysis of two important hadronic QCD processes.

III. IMPLICATIONS FOR $p\bar{p}$ COLLIDER CROSS SECTIONS

At the Fermilab $p\bar{p}$ collider, the jet inclusive cross section is well measured by the CDF Collaboration in the jet p_T range 40–400 GeV/c.[9] The search for the top quark is now focused on the m_t range 90–250 GeV.[14] In perturbative QCD, both these cross sections have contributions from quarks and gluons in the initial state, and both have an overall factor of α_s^2 in lowest order. More importantly from the point of view of *precision* measurements, the next-to-leading-order perturbative corrections for both processes are known.[10,15] In this section we compare the predictions for both cross sections calculated using the five sets of partons derived above. It will turn out that the relative sizes and shapes of the different predictions for the cross section can be completely understood in terms of the relative behavior of (a) the quark and gluon distributions at scales Q and values of $x \sim Q/\sqrt{s}$ and (b) the strong coupling $\alpha_s^2(Q)$, where $Q \sim p_T$ and m_t for jet and $t\bar{t}$ production, respectively.

For reference, therefore, we show in Fig. 5 the quark and gluon distributions as a function of x for the "'typical" value of $Q = 250$ GeV, normalized to the B_0 distributions. The quark distributions are essentially identical at the starting value of $Q_0^2 = 4$ GeV^2, but evolve apart as Q^2 increases, according to the value of $\Lambda_{\overline{\rm MS}}$, as can be seen in Fig. 5(b). The gluon distributions are, of course, already quite different at Q_0, two being harder than B_0, two being softer. There is a crossover point which moves with the QCD evolution from $x \sim 0.1$ at $Q^2 = 5$ GeV^2 to the value $x \sim 0.03$ at $Q = 250$ GeV seen in Fig. 5(a). Figure 6 shows the relative size of the strong coupling $\alpha_s^2(Q)$ as a function of Q. Here the ordering is determined simply by the $\Lambda_{\overline{\rm MS}}$ value.

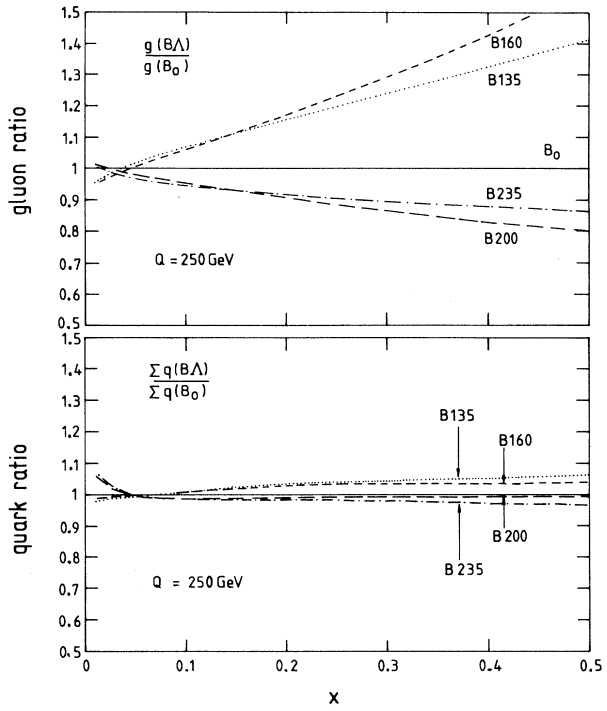

FIG. 5. (a) Gluon and (b) quark distributions as a function of x normalized to B_0 at $Q = 250$ GeV, where $\Sigma q \equiv u + \bar{u} + d + \cdots$.

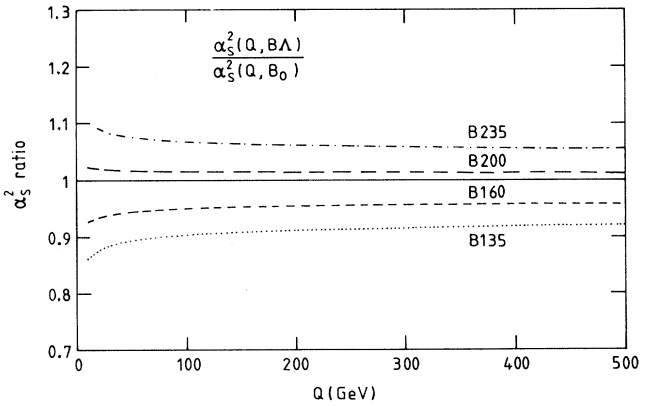

FIG. 6. Values of $\alpha_s^2(Q)$ as a function of Q, for the various $\Lambda_{\overline{\rm MS}}$ values used in the different sets, normalized to that for the B_0 value of $\Lambda^{(4)}_{\overline{\rm MS}} = 190$ MeV.

A. Single jet inclusive p_T distribution

The calculation of the complete next-to-leading-order QCD corrections to the inclusive large p_T jet cross section has been performed recently by Ellis, Kunszt, and Soper.[10]. This allows—for the first time—a *precision* comparison of theory with data. Already, impressive agreement has been demonstrated with data from the CDF Collaboration.[9] (See, for example, Fig. 3 of Ref. 10.) For the first time, therefore, there is the very real possibility of using the jet data to obtain information on the parton distributions—especially the gluon distribution—and $\Lambda_{\overline{\rm MS}}$. The distributions derived above are ideal for investigating this question. Note that the HMRS(B) distributions,[7] which are essentially identical to the B_0 distributions in the range of x being considered, are already known to give excellent agreement with the data.[10] The question then is whether the spread in predictions from the other four sets is large enough for them to be distinguished by the data.

Since our purpose here is to explore the potential of the jet data for measuring the gluon and $\Lambda_{\overline{\rm MS}}$, we do not attempt to repeat the exact next-to-leading-order analysis of Ref. 10. Instead, we notice from Fig. 2 in Ref. 10 that for the typical CDF jet transverse momenta and cone size the scale dependence is rather weak, and so the largest theoretical uncertainties will come from the value of $\Lambda_{\overline{\rm MS}}$ and the gluon. From the same figure in Ref. 10 we also notice that the exact next-to-leading-order result can be well approximated by the leading-order expression evaluated at scale $\mu = p_T$. Certainly as far as *ratios* of cross sections are concerned, this approximation is perfectly acceptable. Figure 7 shows the spread in the predictions of the inclusive jet p_T distribution at jet rapidity $\eta = 0$ and $\sqrt{s} = 1.8$ TeV arising from all five sets. For reference the numerical values of the cross section using the

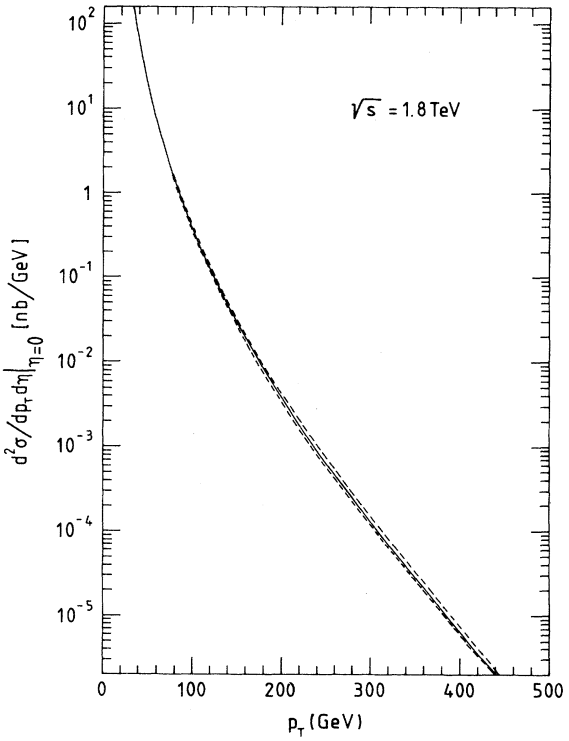

FIG. 7. Jet p_T distribution at $\eta = 0$ and $\sqrt{s} = 1.8$ TeV, showing the B_0 prediction and the total spread from using the other sets of partons. The cross-section values predicted by the B_0 set of partons are tabulated in Table II.

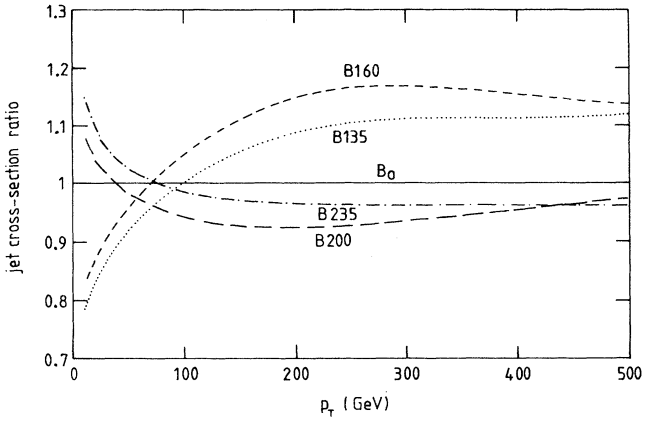

FIG. 8. As for Fig. 7, but shown for all four sets normalized to the B_0 prediction.

TABLE II. Numerical values of the inclusive jet cross section at $\eta = 0$, $\sqrt{s} = 1.8$ TeV using the B_0 set of partons at leading order with scale $\mu = p_T$.

p_T (GeV/c)	$d^2\sigma/dp_T d\eta\|_{\eta=0}$ (nb/GeV c^{-1})
20	0.184×10^{4}
40	0.653×10^{2}
60	0.770×10^{1}
80	0.152×10^{1}
100	0.403×10^{0}
120	0.129×10^{0}
140	0.469×10^{-1}
160	0.188×10^{-1}
180	0.814×10^{-2}
200	0.373×10^{-2}
220	0.179×10^{-2}
240	0.892×10^{-3}
260	0.458×10^{-3}
280	0.241×10^{-3}
300	0.129×10^{-3}
320	0.700×10^{-4}
340	0.384×10^{-4}
360	0.212×10^{-4}
380	0.117×10^{-4}
400	0.649×10^{-5}
420	0.358×10^{-5}
440	0.197×10^{-5}
460	0.107×10^{-5}
480	0.577×10^{-6}
500	0.306×10^{-6}

B_0 prediction are tabulated in Table II.

More interesting is Fig. 8, which shows the same cross sections normalized to that of B_0. We note the following points.

(i) The spread overall is less than $\pm 20\%$.

(ii) There are two distinct p_T ranges: for $p_T \lesssim 200$ GeV/c the cross section is dominated by the gg and qg scattering subprocesses. [See, for example, Fig. 5(a) of Ref. 16.] Here the cross-section ratios reflect the relative shapes of the gluon distributions, i.e., the steepness of the cross section increases with increasing η_g—compare Fig. 5(a) with Fig. 8. The cross sections are further separated to some extent by the differences between the corresponding α_s^2 (Fig. 6).

(iii) For $p_T \gtrsim 200$ GeV/c the quark-initiated processes become more important and the *shapes* of the cross sections become more similar. It is interesting, however, that the cross sections are *not* ordered according to the size of α_s^2. This is because there is still a substantial contribution from the qg scattering subprocess and also because it is the distributions with the smaller $\Lambda_{\overline{\rm MS}}$ which evolve more slowly and consequently have larger quark and gluon distributions at medium and large x.

It is likely that ultimately the *shape* of the jet cross section will be measured much more precisely than the *normalization*. We see from Fig. 8 that for $p_T \gtrsim 200$ GeV/c the shape is rather precisely predicted, but there is no simple correlation between the size of the cross section and the value of $\Lambda_{\overline{\rm MS}}$. On the other hand, for p_T values in the 40–200 GeV/c range an experimental accuracy of about 5% or less on the shape will provide a rather good discrimination of the shape of the gluon distribution in the x range 0.05–0.2. Comparing Figs. 4 and 8, there is no reason why the gluon discriminating power cannot be comparable or even better than the fixed-target prompt-photon data. The way to proceed is to first calculate the exact next-to-leading cross section using these five distributions and then to calculate the χ^2 for the fit to the CDF data in this range as a function of the (assumed unknown) overall normalization factor. Comparisons of the minimum χ^2 for each set (assuming the "best fit" normalization factor is consistent with the quoted experimental systematic uncertainty on the normalization) will then determine the preferred value and error for η_g.

B. Top-quark cross sections

Recent results from the CDF collaboration at the Fermilab $p\bar{p}$ collider[14] and from CERN e^+e^- collider LEP[17] have placed the (standard model) top-quark mass (m_t) in the 90–200-GeV range. This implies that the top quark could well be discovered at the FNAL $p\bar{p}$ collider in the next few years. Since the production cross sections are rather small for top masses in this range, it will *not* be possible to measure m_t from a fit to the final-state lepton spectrum, as is done, for example, for the W boson. Instead the mass measurement, or mass limit if no events are observed, will have to rely on a comparison of the theoretical and experimental cross sections as a function of m_t. In this way, the present CDF 95%-C.L. limit of 89 GeV (Ref. 14) is obtained using the theoretical cross sections of Altarelli *et al.*,[18] which were based on the next-to-leading-order calculation of the total cross section by Nason, Dawson, and Ellis,[15] and the Diemoz-Ferroni-Longo-Martinelli (DFLM) parton distributions.[19] It is already clear that a precise measurement of the top-quark mass is absolutely necessary for extracting information on the Higgs-boson mass from detailed electroweak phenomenology.[17] A significant part of the uncertainty from a collider measurement of m_t will come from the uncertainty in the theoretical cross section. Previous attempts to gauge this[15,18] have focused on two sources of uncertainty: (a) the uncertainty due to the parton distributions, and (b) the uncertainty due to unknown higher-order perturbative corrections, as parametrized by varying the renormalization and/or factorization scale in the next-to-leading-order calculation.

We believe that the parton distributions are now more tightly constrained than has previously been suggested. Furthermore, it is now possible to derive a quantitative error for the theoretical prediction, based on the range of allowed values of $\Lambda_{\overline{\rm MS}}$ and the gluon described above. Our strategy is therefore as follows. We use the B_0 distributions as our "best guess" parton distributions and calculate the cross section for $t\bar{t}$ production as a function of m_t. We then repeat the calculation using the other four distributions, to derive a band of uncertainty, in the same way as for the jet cross section. Unlike the latter, however, the top cross section has a nontrivial residual dependence on μ, the (assumed equal) factorization and renormalization scale. Traditionally[15,18] the uncertainty is gauged by allowing μ to vary in the range $m_t/2 < \mu < 2m_t$, with $\mu = m_t$ taken as the central value. The logic for this is as follows. For a given m_t the cross section is maximal for the "optimization scale," $\mu = \mu_{\rm opt}$. In the relevant range of top masses, it is found that, to a good approximation,[16]

$$\mu_{\rm opt} = 0.2\left(1 + \frac{m_t}{100\ \text{GeV}}\right) m_t, \tag{3}$$

and so $\mu_{\rm opt}/m_t$ varies from 0.4 to 0.6 as m_t varies from 100 to 200 GeV. The scale choice $\mu = m_t/2$ therefore provides a reasonable *upper* bound on the theoretical cross section. In a similar way it is found that the cross section decreases for $\mu > \mu_{\rm opt}$, and the choice $\mu = 2m_t$ gives a cross section roughly as far below $\mu = m_t$ as $\mu = \mu_{\rm opt}$ is above. The effect is apparent in the cross sections calculated below.

The dashed curves in Fig. 9 embrace the spread of the predictions for the total $t\bar{t}$ cross section calculated using the five sets of partons and the three scales. The upper dashed line corresponds to set B160 with $\mu = m_t/2$, the central solid line to set B_0 with $\mu = m_t$, and the lower dashed line to set B200 with $\mu = 2m_t$. For reference, the numerical values of the cross sections shown in Fig. 9 are

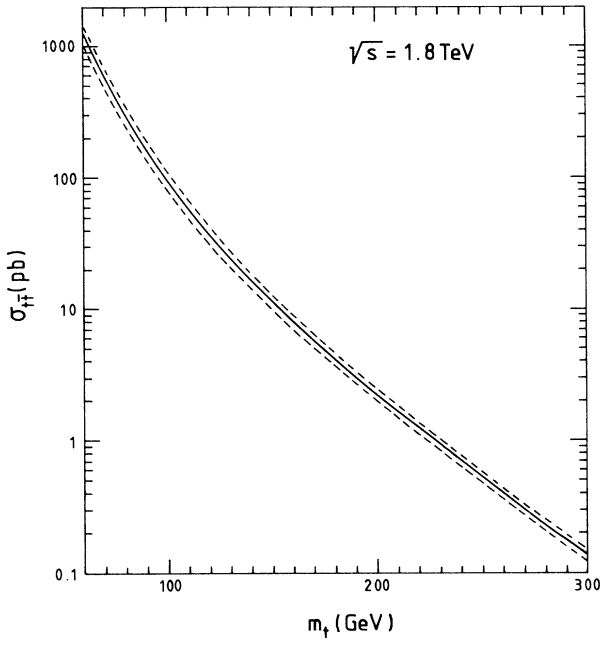

FIG. 9. Predictions for top-quark production ($\sigma_{t\bar{t}}$) as a function of m_t at $\sqrt{s} = 1.8$ TeV. The continuous curve is the B_0 ($\mu = m_t$) prediction, and the dashed curves embrace all the other predictions. The cross-section values are listed in Table III.

TABLE III. Numerical values of the top-quark cross sections shown in Fig. 9.

	$\sigma_{t\bar{t}}$ (pb)		
m_t (GeV)	B160, $\mu = m_t/2$	B_0, $\mu = m_t$	B200, $\mu = 2m_t$
60	1455	1282	1048
80	348	299	246
100	110	95.0	79.1
120	42.3	36.9	31.3
140	18.5	16.4	14.1
160	8.87	7.97	6.99
180	4.54	4.13	3.66
200	2.43	2.23	1.98
220	1.35	1.25	1.11
240	0.763	0.705	0.625
260	0.437	0.405	0.359
280	0.253	0.235	0.207
300	0.147	0.136	0.120

tabulated in Table III.

Figure 10 shows all 15 predictions normalized to the central (B_0) prediction of Fig. 9. A clear trend is evident. At m_t values less than about 100 GeV the cross section is dominated by gluon fusion, i.e., $gg \to t\bar{t}$ (see Fig. 12 of Ref. 16). The shapes of the curves here reflect the shapes of the different gluons. Note that although naively one might expect that the "typical" parton x probed is of order $2m_t/\sqrt{s}$, the fact that the top quarks have additional kinetic energy of the order of their mass leads to a higher mean value, $x \sim 4m_t/\sqrt{s}$. Superimposed on the shape differences are the effects of the different $\Lambda_{\overline{\rm MS}}$ values in the overall α_s^2 couplings. For m_t values higher than 100 GeV there is a transition from gluon-fusion dominance to quark-fusion dominance, i.e., $q\bar{q} \to t\bar{t}$, and the cross sections converge. For a given choice of scale μ, one might expect that the ordering at large m_t is simply that of the $\Lambda_{\overline{\rm MS}}$ values. However, once again we see the importance of the QCD evolution of the distributions. As shown in Fig. 5(b) the sets with the smallest $\Lambda_{\overline{\rm MS}}$ evolve slowest and therefore have relatively larger quark distributions at large x. From Figs. 5(b) and 6 we see that the effect is large enough at large m_t to counterbalance the effects of the overall α_s^2. The result is that for a given scale choice the predictions are *not* always ordered according to the $\Lambda_{\overline{\rm MS}}$ value. The net spread for a given choice of μ is only of the order of a few percent. To a first approximation, changing the scale just shifts the curves up and down uniformly. Because the variation of μ is allowed to be more severe than that of $\Lambda_{\overline{\rm MS}}$ (a factor of 4 compared to a factor of about 2), at large m_t it is the scale dependence that provides the dominant uncertainty.

At present we can regard the overall variation shown in Fig. 10—between ±10% and ±15%—as giving the typical theoretical uncertainty. Although the uncertainty

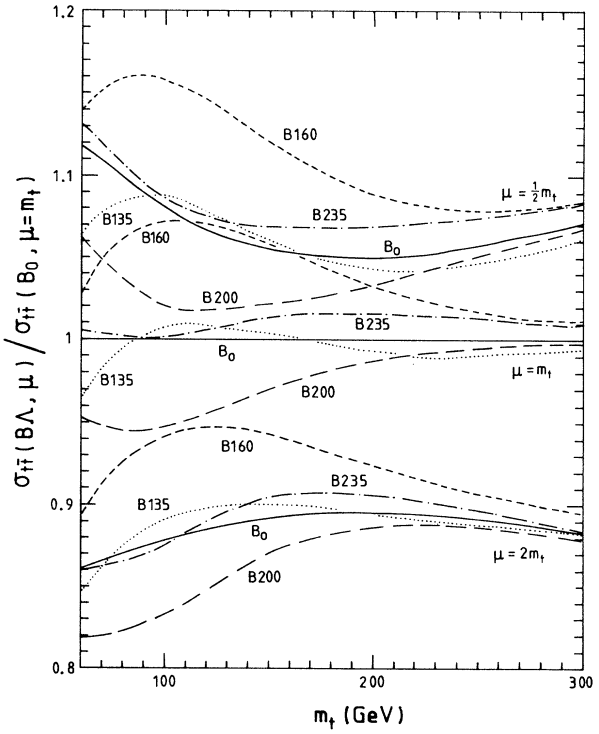

FIG. 10. The predictions for the top-quark cross section, normalized to B_0 ($\mu = m_t$), obtained from the five sets of partons for three different scales: $\mu = \frac{1}{2}m_t$, m_t, $2m_t$.

on the *cross section* decreases as m_t increases, it is remarkable that the corresponding uncertainty on m_t for a given cross section stays roughly constant. This is because the cross section becomes less steep as a function of m_t as the latter increases. Returning to Fig. 9, we see that the horizontal width of the band is constant at about 8 GeV over the whole range, and approximately symmetric about the central B_0 prediction. This, then, gives an error of ± 4 GeV in the determination of the top mass arising from the theoretical uncertainty in the QCD prediction of the cross section, using B_0 ($\mu = m_t$) as the "best guess" prediction. Note that in a sense we have added the two errors (scale and parton distributions) *linearly* rather than in *quadrature*, thus giving a more conservative uncertainty.

One way to reduce this error would be to use the inclusive jet cross section to *calibrate* the top cross section. In fact a precise measurement of the jet cross section could, in principle, essentially eliminate the error due to the parton distributions, by picking out a preferred curve on Fig. 7. Unfortunately, this would not remove the scale uncertainty, which would remain at roughly $\pm 10\%$ over the whole mass range.

Finally, if we compare our results on the top-quark cross section (Fig. 9) with the earlier results of Altarelli *et al.* (for example, Table 2 of Ref. 18), we find that while the predicted cross sections are similar in magnitude for top-quark masses of order 100 GeV or less, our cross sections are significantly higher at larger m_t. To investigate the reason for this we recall that Altarelli *et al.*[18] used the DFLM partons of Ref. 19. Now if we compare the predictions we obtain using the (central) set of DFLM partons ($\Lambda^{(4)}_{\overline{\rm MS}} = 260$ MeV, $\mu = m_t$) with those using our B_0 set ($\Lambda^{(4)}_{\overline{\rm MS}} = 190$ MeV, $\mu = m_t$) we indeed find that the former are lower by 5%, 16% at $m_t = 80$, 200 GeV, respectively. We believe that this is because our quark distributions are larger at medium and large x than those of DFLM. A very clear illustration of this is provided by Fig. 11, which shows the structure function $F_2^{\mu p}$ at $Q^2 = 20$ GeV^2 corresponding to the B_0 and DFLM sets of partons. The data—from the BCDMS Collaboration[2] (rescaled by 0.98 as suggested by the SLAC data)—clearly favor the former.

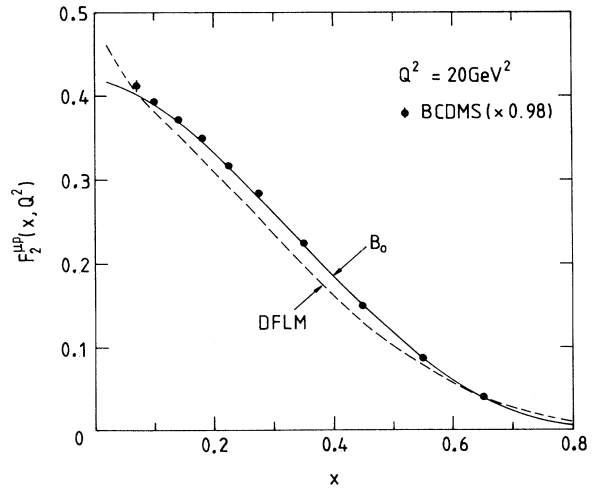

FIG. 11. The structure function $F_2^{\mu p}$ at $Q^2 = 20$ GeV^2 from the BCDMS Collaboration (Ref. 2) (scaled by 0.98, see text). The curves correspond to the B_0 (Ref. 8) (solid line) and Diemoz *et al.* (Ref. 19) (DFLM, $\Lambda^{(4)}_{\overline{\rm MS}} = 260$ MeV) (dashed line) parton distributions.

IV. CONCLUSIONS

Our knowledge of QCD processes continues to increase both experimentally and theoretically. Deep-inelastic lepton-nucleon scattering processes are now measured with high-precision. In addition, experiments at the high-energy $p\bar{p}$ colliders have enabled a variety of QCD processes to be studied over a much wider kinematic regime. On the theoretical side, next-to-leading-order contributions are now known for almost all the relevant QCD processes, which allows much more accurate predictions to be made. Global next-to-leading-order analyses of the deep-inelastic scattering and related data have enabled a definitive set of parton distributions to be obtained, at least in the region $0.03 \lesssim x \lesssim 0.6$ relevant to current data. In this region the parton sets HMRS(B) and KMRS(B_0,B_-) are only marginally different. To be definite we have here used set B_0 as the standard. (Of course if we were to extrapolate into the unexplored very small x region we would also have to consider the B_- set of partons.) In addition to deep-inelastic scattering, these distributions are in remarkable agreement with a wide body of data, including prompt photon production, Drell-Yan and W, Z production, and jet production. Taken together this is a significant confirmation of QCD.

In this paper we have attempted to quantify as carefully as possible the uncertainties in the QCD predictions associated with the parton distributions. We have presented four sets of distributions which are equally acceptable and which span the uncertainty in our optimum B_0 set of partons. At the same time we have studied the uncertainty in the determination of $\Lambda_{\overline{\rm MS}}$. To do this we repeated the global analysis of the deep-inelastic scattering and prompt-photon data for different fixed values of $\Lambda_{\overline{\rm MS}}$ and the strongly correlated parameter η_g [the exponent of $(1-x)$ in the gluon distribution]. The results were presented in Figs. 1 and 2 and confirm[7,13] that *both* deep-inelastic scattering and prompt-photon data are needed to pin down the two parameters. To be precise, we found that acceptable sets of partons exist for values of these two parameters lying within an ellipselike region in the $\Lambda^{(4)}_{\overline{\rm MS}}$, η_g plane bounded by

$$\Lambda^{(4)}_{\overline{\rm MS}} = 185 \pm 50 \text{ MeV}, \qquad \eta_g = 4.95 \pm 0.7. \tag{4}$$

We argued that this represents the optimum determination of $\Lambda^{(4)}_{\overline{\rm MS}}$ from existing deep-inelastic scattering and related data, and corresponds to

$$\alpha_s(M_Z) = 0.109^{+0.004}_{-0.005}. \quad (5)$$

We note that the value of $\Lambda^{(4)}_{\overline{\rm MS}}$ in Eq. (4) is in good agreement with the determination $\Lambda^{(4)}_{\overline{\rm MS}} = 205 \pm 22(\text{stat}) \pm 60(\text{syst})$ MeV obtained by the BCDMS Collaboration[20] using only their own data in the high-x region. Of course without prompt-photon data they are unable to determine η_g as precisely as that quoted in Eq. (4); using just their own $F_2^{\mu p}$ data (but in the whole x region) they find $\eta_g = 8.0 \pm 1.5(\text{stat}) \pm 2.0(\text{syst})$. The effect of this increased uncertainty in η_g can be estimated from the dashed curves in Fig. 3, which compare our optimum determination of $\Lambda^{(4)}_{\overline{\rm MS}} = 180$ MeV, $\eta_g = 10$ from fitting to BCDMS $F_2^{\mu p}$ data alone, with a similar fit (giving $\Lambda^{(4)}_{\overline{\rm MS}} = 220$ MeV) in which η_g is fixed at the more realistic value $\eta_g = 5$.

To quantify the error on the QCD predictions arising from the parton distributions we used the four sets B135, B160, B200, and B235, with values of $\Lambda^{(4)}_{\overline{\rm MS}}$ and η_g at their limits of acceptability as shown by the dots in Figs. 1 and 2. We explicitly considered the uncertainties in the predictions of the jet inclusive p_T distribution (Figs. 7 and 8) and of the cross section for $t\bar{t}$ production (Figs. 9 and 10) in $p\bar{p}$ collisions at $\sqrt{s} = 1.8$ TeV. For the former process, we showed that accurate measurements of the shape of the cross section in the 40–200 GeV/c p_T range should help constrain the gluon distribution, at a level comparable to that of the prompt-photon fixed-target data. For the latter process, the uncertainty in the theoretical predictions would translate into a ± 4 GeV error on the determination of the mass of the top quark if the rate of $t\bar{t}$ production were measured at the Fermilab Tevatron.

ACKNOWLEDGMENTS

We are grateful to J. Ellis, R. K. Ellis, and S. D. Ellis for useful discussions. This work was supported in part by the University of Washington and by the U.S. Department of Energy, Contract No. DE-AS06-88ER40423.

*Permanent address: Departments of Physics and Mathematical Sciences, University of Durham, Durham, England.

[1] A.D. Martin and W.J. Stirling, Phys. Lett. B **237**, 551 (1990).

[2] Bologna-CERN-Dubna-Munich-Saclay (BCDMS) Collaboration, A.C. Benvenuti *et al.*, Phys. Lett. B **223**, 485 (1989).

[3] CERN-Dortmund-Heidelberg-Saclay-Warsaw (CDHSW) Collaboration, J. P. Berge *et al.*, Z. Phys. C **49**, 187 (1991).

[4] European Muon Collaboration (EMC), J. J. Aubert *et al.*, Nucl. Phys. **B259**, 189 (1985).

[5] WA70 Collaboration, M. Bonesini *et al.*, Z. Phys. C **38**, 371 (1988).

[6] E605 Collaboration, C. N. Brown *et al.*, Phys. Rev. Lett. **63**, 2637 (1989).

[7] P. N. Harriman, A. D. Martin, R. G. Roberts, and W. J. Stirling, Phys. Rev. D **42**, 798 (1990).

[8] J. Kwiecinski, A. D. Martin, R. G. Roberts, and W. J. Stirling, Phys. Rev. D **42**, 3645 (1990).

[9] Collider Detector at Fermilab (CDF) Collaboration, F. Abe *et al.*, Phys. Rev. Lett. **62**, 613 (1989); CDF Collaboration, T. L. Hessing, in *High Energy Hadronic Interactions*, proceedings of the XXVth Rencontres de Moriond, Les Arcs, France, 1990, edited by J. Tran Thanh Van (Editions Frontieres, Gif-sur-Yvette, 1990).

[10] S.D. Ellis, Z. Kunszt, and D.E. Soper, Phys. Rev. Lett. **64**, 2121 (1990).

[11] L. Whitlow *et al.*, in *Proceedings of the International Europhysics Conference on High Energy Physics*, Madrid, Spain, 1990, edited by F. Barreiro and C. Lopez (North-Holland, Amsterdam, 1990), p. 215.

[12] New Muon Collaboration (NMC), D. Allasia *et al.*, Phys. Lett. B **294**, 366 (1990); Bologna-CERN-Dubna-Munich-Saclay (BCDMS) Collaboration, A. C. Benvenuti *et al.*, *ibid.* **237**, 599 (1990); European Muon Collaboration (EMC), J. J. Aubert *et al.*, Nucl. Phys. **B293**, 740 (1987).

[13] P. Aurenche, R. Baier, M. Fontannaz, J. F. Owens, and M. Werlen, Phys. Rev. D **39**, 3275 (1989).

[14] CDF Collaboration, F. Abe *et al.*, Report No. FERMILAB-Pub-90/137-E, 1990 (unpublished).

[15] P. Nason, S. Dawson, and R. K. Ellis, Nucl. Phys. **B303**, 607 (1988); W. Beenakker *et al.*, Phys. Rev. D **40**, 54 (1989).

[16] A.D. Martin, R.G. Roberts, and W.J. Stirling, Z. Phys. C **42**, 277 (1989).

[17] See, for example, J. Ellis and G.L. Fogli, Phys. Lett. B **249** 543 (1990).

[18] G. Altarelli, M. Diemoz, G. Martinelli, and P. Nason, Nucl. Phys. **B308**, 724 (1988).

[19] M. Diemoz, F. Ferroni, E. Longo, and G. Martinelli, Z. Phys. C **39**, 21 (1988).

[20] Bologna-CERN-Dubna-Munich-Saclay (BCDMS) Collaboration, A. C. Benvenuti *et al.*, Phys. Lett. B **223**, 490 (1989).